Carbon 177 (2021) 181–188

Contents lists available at ScienceDirect

Carbon

journal homepage: www.elsevier.com/locate/carbon

Research Article

Self-standing carbon nanotube aerogels with amorphous carbon coating as stable host for lithium anodes

Jing Wang [a], Haowen Liu [a], Hengcai Wu [a], Qunqing Li [a, b], Yuegang Zhang [a, b], Shoushan Fan [a], Jiaping Wang [a, b, *]

[a] Department of Physics and Tsinghua-Foxconn Nanotechnology Research Center, Tsinghua University, Beijing, 100084, China
[b] Frontier Science Center for Quantum Information, Beijing, 100084, China

ARTICLE INFO

Article history:
Received 18 January 2021
Received in revised form
6 February 2021
Accepted 18 February 2021
Available online 24 February 2021

Keywords:
Lithium-ion battery
Lithium metal anode
Carbon nanotubes aerogel
Thermal infusion

ABSTRACT

Lithium metal anodes have a high theoretic capacity and are considered the promising electrodes for high energy density rechargeable batteries. However, the uneven deposition of lithium and lithium dendrites hinders the practical usage of lithium metal anodes. In order to solve this problem, carbon nanotube aerogels coated with amorphous carbon (AC@CNT aerogels) are used as the host, and molten lithium infuses into the carbon aerogels to obtain composite lithium metal anodes. The self-standing, porous AC@CNT aerogels provide a solid structure for lithium deposition/stripping and effectively reduce the local current density, so that lithium dendrites are suppressed and better electrochemical performances are achieved. Compared with the bare lithium metal anodes, the AC@CNT aerogel/lithium metal (AC@CNT/Li) anodes exhibit a longer cycling life of 500 h at deposition/striping capacity of 1 mAh cm^{-2} on symmetric cells, better cycling performance of 152 mAh g^{-1} at 0.1C in lithium cobalt oxide/lithium (LCO/Li) cells, and 120.3 mAh g^{-1} at 1 C in lithium iron phosphate/Li (LFP/Li) cells, demonstrating the potential of the AC@CNT/Li electrodes in developing high-performance lithium-metal batteries.

1. Introduction

Lithium-ion batteries are widely used in electric vehicles, portable electronic devices, and so on. The anode of the conventional lithium-ion batteries is graphite, and the theoretic capacity is 372 mAh g^{-1}, which cannot meet the increased demands for higher capacity. Lithium (Li) metal anode is considered a solution due to its high theoretic capacity of 3860 mAh g^{-1} and low redox potential of −3.04 V [1,2]. However, lithium metal anode suffers some problems that hinder its practical applications [3–8]. The deposition of the lithium is uneven during cycling, leading to the growth of lithium dendrites. The chemical reactions between lithium and liquid electrolyte cause the formation of the solid electrolyte interface (SEI) on the lithium metal surface. The uneven lithium deposition and lithium dendrites break the SEI and the fresh lithium under the SEI reacts with the liquid electrolyte, leading to further electrolyte consumption and side reaction. The structure of the lithium metal anode becomes loose, and volume change occurs with the formation of new SEI and growth of lithium dendrites. These problems eventually cause capacity loss, low coulombic efficiency, and a high risk of battery failure.

In general, there are some strategies to solve the problems of the Li anodes: (i) adding additives such as lithium nitrate, $CsPF_6$, and $RbPF_6$ to the electrolyte to regulate the lithium deposition [9–11]. (ii) applying solid electrolyte or gel electrolyte to prevent the growth of lithium dendrites [12,13]. (iii) designing an artificial layer at the electrode/electrolyte interface for dendrite suppression [14,15]. (iv) applying a three-dimensional (3D) structure as the "host" for lithium metal to modulate lithium deposition [16–22]. Among these strategies, the 3D structural host has the advantage of a large contact surface, which can lower the local current density on the anode surface. The 3D structural host can also adapt to the volume change of lithium during cycling. For example, various metal and carbon materials have been used as the host to combine with the lithium metal. Carbon materials such as mesoporous carbon, CNT, and graphene have high surface areas with excellent mechanical strength and flexibility and are the ideal host candidates for lithium metal anode. Carbon materials also have excellent conductivity and can build a self-standing porous structure with

* Corresponding author. Department of Physics and Tsinghua-Foxconn Nanotechnology Research Center, Tsinghua University, Beijing, 100084, China.
E-mail address: jpwang@tsinghua.edu.cn (J. Wang).

https://doi.org/10.1016/j.carbon.2021.02.075
0008-6223/

low density [23,24,32].

It is essential to pre-store lithium into the electrode for a composite lithium metal anode. There are many ways to combine the host and lithium, such as mechanical combining [25,26] and thermal infusion [20,27]. Ideally, the host materials are lithiophilic for constructing a composite lithium metal, but pure carbon materials are not lithiophilic. Adding lithiophilic materials such as Au and ZnO by sputtering or chemical precipitation method is the most common strategy to improve the lithiophilicity of carbon materials [28–30]. However, the contact between some lithiophilic materials and carbon materials is not firmly, and some materials such as Ag and Au are expensive. Amorphous carbon modification is a feasible way to solve these problems. Amorphous carbon reacts with lithium [31] and helps the combination of the carbon materials and lithium to build a composite lithium metal. Among the carbon materials, CNT can build a self-standing skeleton. Amorphous carbon encapsulates the surface and junction of the CNTs and plays a role in welding the CNTs and stabilizing the structure [23,32].

In this work, CNT aerogels coated with amorphous carbon (AC@CNT aerogels) were used as the host to fabricate lithium metal anodes. The self-standing CNT aerogels were fabricated by freeze-drying and then coated with amorphous carbon. Super-aligned carbon nanotubes (SACNTs) with large aspect ratio ($\approx 10^4$), clean surface, high purity, and strong interaction among tubes were used to fabricate self-standing CNT aerogels by freeze-drying, followed with amorphous carbon coating [23,32]. The AC@CNT aerogels and lithium were combined together by thermal infusion to fabricate composite lithium metal anodes (AC@CNT/Li). The AC@CNT aerogel with a relatively large surface area and stable structure guaranteed uniform lithium infusion during synthesis and lithium deposition/stripping during cycling. The porous structure of the AC@CNT aerogel significantly mitigated the volume change of the lithium anode during cycling. The CNT skeleton provided an electrochemically and mechanically stable interface, leading to the formation of a stable SEI. The AC@CNT/Li electrodes were tested on symmetric cells, lithium cobalt oxide/lithium (LCO/Li) cells, and lithium iron phosphate/Li (LFP/Li) cells. The symmetric cells exhibited a long cycle life of 500 h, the LCO/Li cells displayed a capacity of 152 mAh g^{-1} at 0.1C, and the LFP/Li cells showed a capacity of 120.3 mAh g^{-1} at 1 C, which were superior to the cells with the bare lithium metal anodes.

2. Experimental

2.1. Fabrication of the AC@CNT aerogel

Chemical vapor deposition was applied to synthesize SACNTs, and the tube diameter and height of SACNTS were 10–20 nm and 300 μm, respectively [33–35]. SACNTs were dispersed in ethyl-alcohol by ultra-sonication for 30 min. The mixture was washed with deionized water to remove the ethyl-alcohol and underwent a freeze-drying process to obtain a CNT aerogel with a 3D porous structure and a density of 10 mg cm^{-3}. The CNT aerogel was cut into a cylinder with a diameter of 16 mm, heated at 800 °C in mix atmosphere of nitrogen and acetylene for 10 min to achieve an AC@CNT aerogel.

2.2. Fabrication of the AC@CNT/Li, LCO electrodes, and LFP electrodes

Lithium foil was heated to 300 °C to obtain liquid lithium. Then an AC@CNT aerogel was put on top of the liquid lithium, and the liquid lithium infused into the AC@CNT aerogel, forming an AC@CNT/Li electrode. The composite AC@CNT/Li electrode was pressed by a rolling mill to the required thickness of around 600 μm. The Li mass loading was controlled by the volume and density of the AC@CNT aerogels. The areal loadings of Li were 0.25–0.27 g cm^{-2} and 0.09–0.1 g cm^{-2} before and after pressing, and the mass ratio of Li was about 91–94% in the AC@CNT/Li electrode. The LCO slurry was prepared by mixing LCO, super-P, and poly-(vinyl difluoride) at a weight ratio of 8:1:1 in *N*-methyl pyrrolidone (NMP) and pasted on an aluminum foil. After drying at 120 °C for 24 h, the electrode sheet was cut into discs with a diameter of 10 mm. The areal loadings of LCO in the electrode was 10 mg cm^{-2}. LFP electrodes were prepared in the same way and the areal loading was 7 mg cm^{-2}.

2.3. Characterization

The morphology of the CNT aerogel, AC@CNT aerogel, and AC@CNT/Li electrodes was observed by scanning electron microscopy (SEM, Sirion 200, FEI) and transmission electron microscopy (TEM, Tecnai G2F20, FEI). X-ray photoelectron spectroscopy (XPS) analysis of the AC@CNT/Li electrodes was performed on an X-ray photoelectron spectrometer (ESCALAB Xi+, ThermoFisher Scientific). The Raman spectra of the CNT and AC@CNT aerogels were obtained on a Raman spectrometer (LabRam-HR/VV, JY). The Brunauere-Emmette-Teller (BET) measurements of the CNT and AC@CNT aerogels were performed on a surface area and porosity analyzer (ASAP 2020).

2.4. Electrochemical measurements

Coin-type symmetric cells and half-cells were assembled in a glovebox (M. Braun Inert Gas System Co. Ltd., Germany) in an argon atmosphere. 1 M LiPF6 with 2 wt% VC in EC:DMC: DEC (1:1:1 by volume) was used as the electrolyte. For the symmetric cells, the AC@CNT/Li electrode and bare lithium metal were used as the working and counter electrodes. For the half-cells, the AC@CNT/Li electrode and bare lithium metal were used as the anode. The LCO or LFP electrode was used as the cathode. Galvanostatic performances of the cells were tested by a Land battery system (Wuhan Land Electronic Co., China) at a cut-off voltage of 3.0–4.3 V for LCO cells and 2.0–3.8 V for LFP cells. Electrochemical impedance spectroscopy (EIS) measurements were performed on a galvanostat instrument (Bio-Logic VMP-3).

3. Results and discussion

TEM images in Fig. 1a and b shows the morphology of the CNTs and AC@CNTs. The wall thickness of the CNTs was 3.5 nm. For the AC@CNTs, amorphous carbon layer with a thickness of 3.1 nm was observed on the outer wall of the CNTs, and the wall thickness of the AC@CNTs was 6.6 nm. SEM images in Fig. 1c and d shows the 3D porous structures of the CNT and AC@CNT aerogels, which provided enough space for lithium infusion and deposition. Raman spectra of both CNT and AC@CNT aerogels contained two characteristic bands, D band (1374 cm^{-1}) and G band (1580 cm^{-1}). The defect and amorphous carbon concentration of CNTs can be estimated by the ratio of the intensity of the D band and G band (I_d/I_g) [36]. Fig. 1e showed the I_d/I_g ratio of the CNT aerogel was 0.853. For the AC@CNT aerogel, the intensity of the D band raised, and the I_d/I_g ratio increased to 1.061 due to the amorphous carbon coating on CNTs. A large specific surface area and enough space of the host are the keys to constructing the composite lithium anode. The specific surface areas of the CNT and AC@CNT aerogels were tested by BET, which were 86.82 and 60.12 m^2 g^{-1}, respectively (Fig. 1f). The pore size distributions are revealed in Fig. S1. Both mesopores and micropores were observed in the aerogels, and macropores are dominant. Although the specific surface area and the number of mesopores

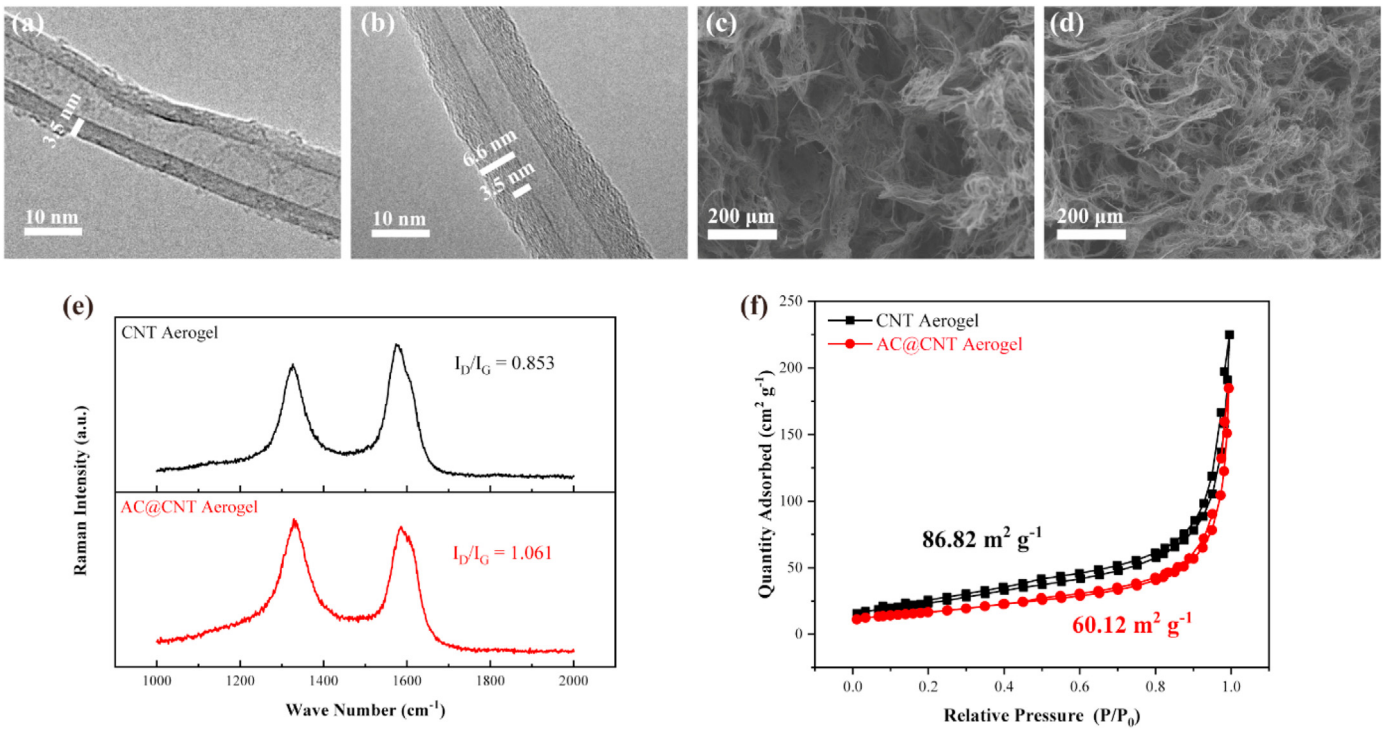

Fig. 1. TEM images of the (a) CNTs and (b) carbon-coated CNTs. SEM images of the (c) CNT and (d) AC@CNT aerogels. (e) Raman spectrum and (f) nitrogen adsorption-desorption isotherms of the CNT and AC@CNT aerogels. (A colour version of this figure can be viewed online.)

and micropores decreased after introducing amorphous carbon coating on CNTs, the AC@CNT aerogel still exhibited a relatively large surface area and could provide enough space to accommodate lithium.

Besides enough space, a stable structure was also important for the construction of the composite lithium metal. Mechanical tests were performed to characterize the structural stability of the CNT and AC@CNT aerogels. As shown in Figs. S2a and S2b, both CNT and AC@CNT aerogels were pressed to a thin film for a few seconds. After removing the pressure, the CNT aerogel remained at the thin film state, while the AC@CNT aerogel recovered to its original form. Furthermore, 200 μL electrolyte was dropped onto the aerogels (Figs. S2c and S2d). The AC@CNT aerogel kept fluffy, while the CNT aerogel collapsed after adding the electrolyte. These tests suggest the more stable structure of the AC@CNT aerogel. The amorphous carbon covered the surface of the CNTs, weld the inter-tube junctions, separated CNTs to prevent agglomeration, and improved the mechanical stability of the CNT aerogel [32].

Fig. 2a and b shows the fabrication procedure of the AC@CNT/Li electrode. The AC@CNT aerogel was put on top of the molten lithium. The molten lithium slowly infiltrated into the aerogel from the bottom and eventually filled the entire AC@CNT aerogel. To characterize the lithium wettability, molten lithium was placed on the CNT and AC@CNT aerogels (Fig. S3). The molten lithium infused into the AC@CNT aerogel in 40 min, but did not infiltrate into the CNT aerogel and the contact angle was 113°, demonstrating the improved lithium wettability of the AC@CNT aerogel as a result of the amorphous carbon coating. To further understand the interaction between lithium and amorphous carbon, the chemical states of Li in the composite lithium metal were characterized by XPS. As shown in Fig. 2c, the spectra showed two peaks. The minor peak at 54.9 eV represented the peak of Li metal. The peak at 55.45 eV was ascribed to the chemical reaction between molten lithium and amorphous carbon [37,38]. During the preparation process of the composite lithium metal electrode, the molten lithium reacted with the amorphous carbon on the aerogel surface first, and then infused into the AC@CNT aerogel slowly and reacted with the inside amorphous carbon. Finally, the molten lithium spread to the entire

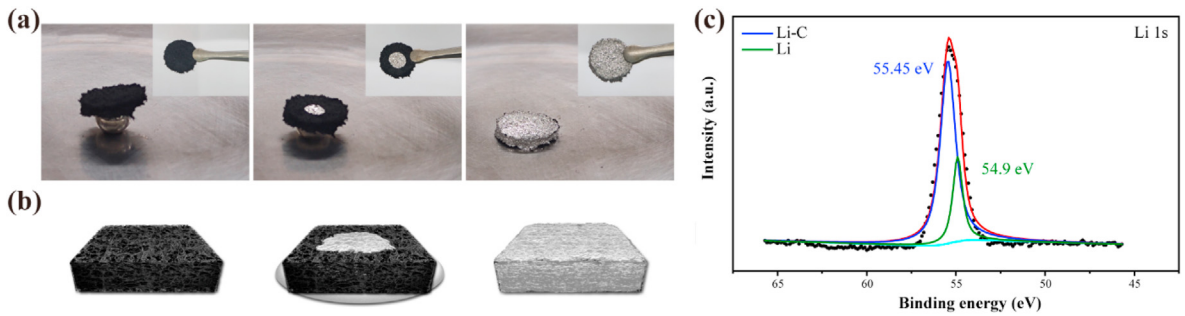

Fig. 2. (a) Photographs and (b) schematic of the fabrication of an AC@CNT/Li electrode. (c) XPS spectra of an AC@CNT/Li electrode. (A colour version of this figure can be viewed online.)

AC@CNT aerogel. The amorphous carbon coating plays an important role in improving the lithium wettability and promoting the infiltration of the molten lithium into the aerogel.

Galvanostatic cycling measurements in symmetrical cells were performed to characterize the electrochemical performances of the bare lithium metal and the AC@CNT/Li electrode. The symmetrical cells were cycled at a fixed current density of 1 mA cm^{-2}, and the deposition/stripping time was 1 h, corresponding to a deposition/stripping capacity of 1 mAh cm^{-2} (Fig. 3a). The voltage profiles at a cycle time of 0–2 h and 78–80 h are shown in Fig. 3b and c. For the AC@CNT/Li electrode, the voltage hysteresis was lower than 0.23 V, which was retained throughout the whole cycle of 500 h. The voltage-time profile of the bare lithium metal showed a gradual voltage hysteresis increase over cycle time. The voltage hysteresis fluctuated irregularly after a cycle time of 90 h due to the uneven deposition of lithium and unstable SEI. A sudden voltage drop occurred at a cycle time of 250 h, which was ascribed to the Li dendrite penetration and the following internal short-circuit. As the current density increased to 2 mA cm^{-2}, the AC@CNT/Li electrode still exhibited lower voltage hysteresis, more stable cycling performance, and longer cell lifetime than the bare lithium metal (Fig. S4). The cycling performances of the symmetric cells were compared with those of Li anodes reported in the literature (Table 1). The AC@CNT/Li electrode exhibited lower voltage hysteresis and longer cycle life than most of the Li anodes in the literature [18,40,41], and showed comparable performances with

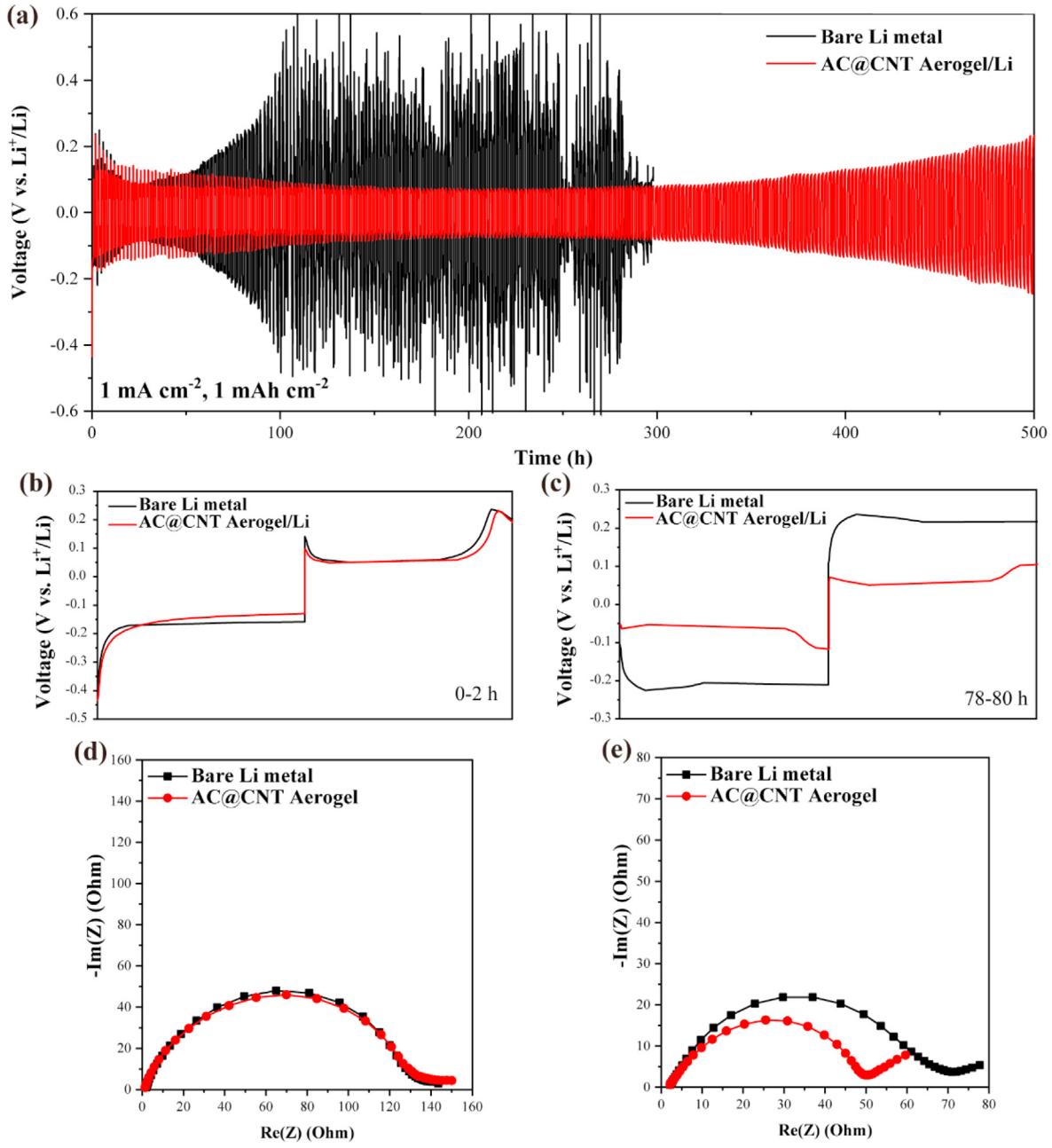

Fig. 3. (a) Galvanostatic cycling performance of the symmetric cells using the bare lithium metal and AC@CNT/Li electrodes at a fixed current density of 1 mA cm^{-2} with a deposition/stripping capacity of 1 mAh cm^{-2}, and the corresponding voltage profiles of the cycles at (b) 0–2 h and (c) 78–80 h, respectively. Nyquist plots of the symmetric cells (d) before cycling and (e) after cycling for 20 h with a deposition/stripping capacity of 1 mAh cm^{-2}. (A colour version of this figure can be viewed online.)

Table 1
Electrochemical properties of symmetric cells of reported lithium metal anode.

	Cycling performances	References
3D Cu mesh	1 mA cm^{-2}, 1 mAh cm^{-2}, 600 h (600 mV)	[18]
	2 mA cm^{-2}, 1 mAh cm^{-2}, 120 h (600 mV)	
CNT + porphyrin	1 mA cm^{-2}, 1 mAh cm^{-2}, 450 h (150 mV)	[39]
Li–In anode	0.5 mA cm^{-2}, 0.5 mAh cm^{-2}, 230 h (200 mV)	[40]
	1 mA cm^{-2}, 1 mAh cm^{-2}, 110 h (500 mV)	
3D carbon fibers + amine (-NH)	1 mA cm^{-2}, 1 mAh cm^{-2}, 500 h (260 mV)	[41]
CNT aerogel + amorphous carbon	1 mA cm^{-2}, 1 mAh cm^{-2}, 500 h (230 mV)	This work
	2 mA cm^{-2}, 1 mAh cm^{-2}, 200 h (310 mV)	

the Li anode based on CNT and porphyrin [39]. The cycling performance differences of the symmetric cells were further testified by EIS analysis before cycling and after 10 cycles at a deposition/stripping capacity of 1 mAh cm^{-2} (Fig. 3d and e). For symmetric cells, the semicircle at the high-frequency range indicates the grain boundary resistance in the SEI and the charge transfer resistance at the lithium surface [5]. Before cycling, the AC@CNT/Li electrode and the bare lithium metal showed a similar interfacial resistance, indicating a similar interface condition. After 10 cycles, the AC@CNT/Li electrode showed smaller impedance than the bare lithium metal. The smaller impedance suggested the more stable SEI and electrode interface, and better lithium deposition/stripping kinetics of the AC@CNT/Li electrode, which was in agreement with the stable voltage-time profile shown in Fig. 3a.

SEM was conducted to compare the surface and cross-sectional morphologies of the bare lithium metal and the AC@CNT/Li electrode after cycling for 100 h in symmetric cells with a deposition/stripping capacity of 1 mAh cm^{-2}. The bare lithium metal showed a rough surface, and there were random cracks and uneven lithium islands (Fig. 4a). For the AC@CNT/Li electrode, the surface was flatter in general with small holes (Fig. 4b). Fig. 4c and d exhibited the cross-section of the bare lithium metal and the AC@CNT/Li electrode. The bare lithium metal underwent a larger volume change, and a 275 μm thick layer of deposited lithium and broken SEI were observed at the top. The curved boundary between the deposited lithium and lithium metal (dotted line in Fig. 4c) suggests the uneven lithium deposition/stripping. The AC@CNT/Li electrode experienced a smaller volume change, and the layer of deposited lithium was thinner (118 μm) and compact, and the boundary between the deposited lithium and lithium metal was much smoother. The loose and unstable structure of the bare lithium metal resulted from the uneven lithium deposition and unstable SEI. The uneven lithium deposition/stripping of the bare lithium metal led to the agglomeration of lithium, which broke the unstable SEI and resulted in random cracks and rough surfaces as shown in Fig. 4a. The electrolyte passed through the SEI from the cracks and reacted with the fresh lithium to form new SEI. The new SEI was unstable, and more electrolyte was consumed. The SEI was formed and broken repeatedly, resulting in a thick layer of deposited lithium and broken SEI with loose structure, and battery failure. After introducing AC@CNT aerogel as a host for lithium metal, the porous AC@CNT aerogel served as a stable skeleton for lithium to reversibly deposit/strip and reduced local current density along the surface of the lithium metal anode. Therefore, the lithium deposited uniformly and compact, and the SEI was intact and stable.

Furthermore, bare lithium metal||bare lithium metal cells and bare lithium metal||AC@CNT/Li cells were assembled using O-ring-shaped separators for better observation of lithium deposition. The assembly method was described in the literature [42]. The O-ring-shaped separator with thickness of 1 mm provided enough space for lithium deposition. The cells were cycled at a current density of 1 mA cm^{-2} for 30 h, and SEM was performed to compare the surface of the bare lithium metal and the AC@CNT/Li electrode. The surface of the bare lithium metal was uneven, and lithium deposits were scattered on the surface (Fig. 4e and f). The structure was loose, and numerous holes were observed. In comparison, the

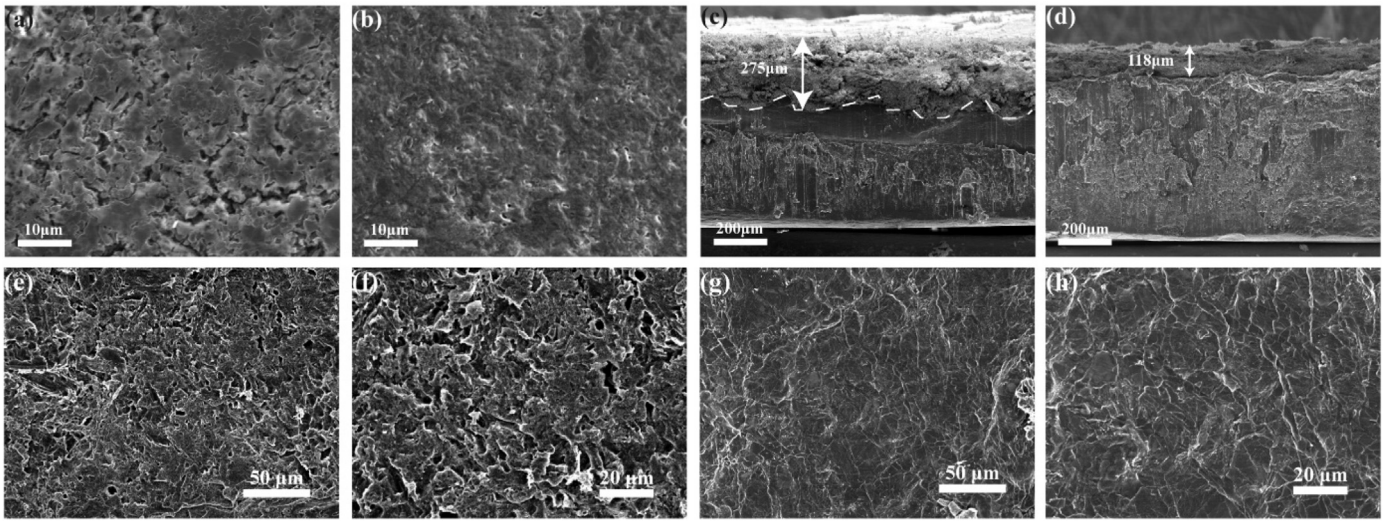

Fig. 4. SEM images of the top surface and cross-sections of the (a, c) lithium metal and the (b, d) AC@CNT/Li anodes after cycling for 100 h in symmetric cells with a deposition/striping capacity of 1 mAh cm^{-2}. SEM images of the top surface of the (e, f) lithium metal and the (g, h) AC@CNT/Li anodes after cycling for 30 h in cells with O-ring-shaped separators with a deposition/striping capacity of 1 mAh cm^{-2}.

surface of the AC@CNT/Li electrode was smoother and lithium deposited uniformly (Fig. 4g and h). The porous AC@CNT aerogel served as a stable skeleton for lithium to reversibly deposit/strip and led to even lithium deposition behavior.

Galvanostatic cycling measurements in LCO cells and LFP cells were also carried out. Fig. 5a showed the cycling performances of LCO cells with the bare lithium metal and AC@CNT/Li anodes. The cells were cycled four times at 0.1C first and 1 C afterward. The LCO cells with the bare lithium metal and AC@CNT/Li anodes exhibited specific capacities of 145.1 mAh g^{-1} and 152.0 mAh g^{-1}, respectively. The cell with the AC@CNT/Li electrode showed an initial capacity of 135.7 mAh g^{-1} at 1 C and 71 mAh g^{-1} after 200 cycles with coulombic efficiency of 99.3%, and the cell with the bare lithium metal anode failed after 182 cycles at 1 C. After the LCO/Li cell with the bare lithium metal failed, the cell was taken apart, and the bare lithium metal anode was replaced with a new bare lithium metal anode. The new LCO/Li cell achieved an initial capacity of 113.2 mAh g^{-1} (Fig. S5). The higher capacity of the new cell than the old cell at the 185th cycle indicated that the decay of the bare lithium metal was the main reason for the battery failure. The rate performances of the LCO cells with the bare lithium metal and AC@CNT/Li anodes are shown in Fig. 5b. The cell with the AC@CNT/Li electrode delivered specific capacities of 165.4, 152.1, 144.3, 137, 126.9, and 108 mAh g^{-1} at 0.1C, 0.2C, 0.5C, 1 C, 2 C, and 5 C, respectively, which were higher than the capacity values of the cell with the bare lithium metal anode. As the cycling rate dropped back to 0.1C, the capacities of the cells with the AC@CNT/Li and bare lithium metal anodes were 164 mAh g^{-1} and 152 mAh g^{-1}, respectively. Fig. 5c shows the cycling performances of LFP cells with the bare lithium metal and AC@CNT/Li anodes at 1 C. The LFP cell with the AC@CNT/Li anode showed an initial capacity of 120.3 mAh g^{-1} and capacity of 92.4 mAh g^{-1} after 300 cycles, corresponding to a capacity retention of 76.8%. The LFP cell with the bare lithium metal delivered an initial capacity of 113.6 mAh g^{-1} and its capacity and the coulombic efficiency drastically decreased after 229 cycles. Fig. 5d showed the rate performances of the LFP cells with the bare lithium metal and AC@CNT/Li anodes. The capacity values of the cell with the AC@CNT/Li were 155.9, 147.7, 136.3, 127.9, 118.1, and 101.1 mAh g^{-1} at 0.1C, 0.2C, 0.5C, 1C, 2C, and 5C, showing superior rate performance than the cell with the bare lithium metal anode. The cycling performances of the LFP and LCO cells were compared with data reported in the literature (Table 2). The LFP cell with the AC@CNT/Li anode showed longer cycle life than that in Ref. [39], and exhibited similar initial capacity at a much higher LFP loading with that in Ref. [43]. The LCO cell with the AC@CNT/Li anode with higher LCO loading and higher rate delivered comparable cycling performance with those in the literature [44,45]. The better galvanostatic performances of the cell with the AC@CNT/Li electrode than that with bare lithium metal demonstrated its potential in developing practical lithium-metal batteries.

4. Conclusion

In this work, composite lithium anodes were fabricated by infiltrating molten lithium into AC@CNT aerogels via thermal infusion. The AC@CNT aerogels showed a stable structure, and amorphous carbon interacted with the molten lithium to facilitate the entire lithium infusion into the AC@CNT aerogels. The porous AC@CNT aerogel provided a robust skeleton and enough space for

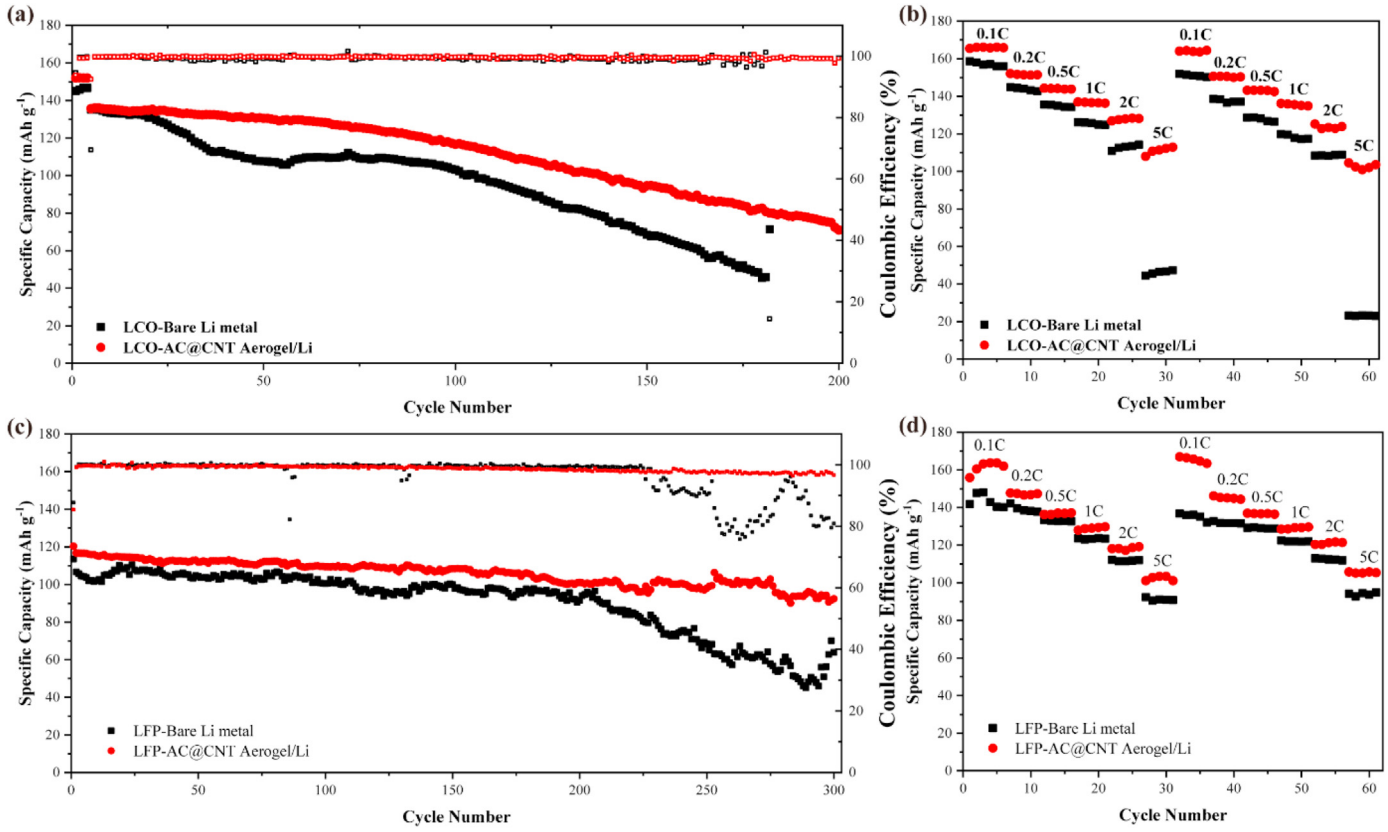

Fig. 5. (a) Cycling and (b) rate performances of LCO cells and (c) cycling and (d) rate performances of LFP cells with the bare lithium metal and AC@CNT/Li anodes. (A colour version of this figure can be viewed online.)

Table 2
Electrochemical properties of LFP cells and LCO cells of reported lithium metal anodes.

	Cycling performances of LFP cells	Cycling performances of LCO cells	References
CNT + porphyrin	7.6 mg cm^{-2} 124 mAh g^{-1} (1 cycle, 1C) 99.3 mAh g^{-1} (100 cycles, 1C)	/	[39]
3D Multichannel carbon fibers + Ag	4 mg cm^{-2} 120 mAh g^{-1} (1 cycle, 1C) 110 mAh g^{-1} (600 cycles, 1C)	/	[43]
3D porous CeO_2 ceramic host	/	3 mg cm^{-2} 143 mAh g^{-1} (1 cycle, 0.2C) 112 mAh g^{-1} (125 cycles, 0.2C)	[44]
Multi-walled carbon nanotube	/	12.8 mg cm^{-2} 134 mAh g^{-1} (1 cycle, 0.1C) 98.7 mAh g^{-1} (200 cycles, 0.5C)	[45]
CNT aerogel + amorphous carbon	7 mg cm^{-2} 120.3 mAh g^{-1} (1 cycle, 1C) 92.4 mAh g^{-1} (300 cycles, 1C)	10 mg cm^{-2} 152 mAh g^{-1} (1 cycle, 0.1C) 135.7 mAh g^{-1} (5 cycles, 1C) 71 mAh g^{-1} (200 cycles, 1C)	This work

lithium deposition/stripping and reduced the current density along the surface of the lithium metal anode. As a result, the symmetric cells with AC@CNT/Li electrodes exhibited a long cycling life of 500 h at deposition/stripping capacity of 1 mAh cm^{-2}, the LCO cells with the AC@CNT/Li anodes displayed an initial capacity of 152 mAh g^{-1} at 0.1C, and LFP cells with the AC@CNT/Li anodes showed a capacity of 120.3 mAh g^{-1} with a capacity retention of 76.9% after 300 cycles. The SEM results revealed stable SEI layer and better deposition/stripping behavior on the surface of the AC@CNT/Li electrode, suggesting a promising option for fabricating reliable lithium metal anodes for high-energy and high-power lithium battery systems.

CRediT authorship contribution statement

Jing Wang: Conceptualization, Investigation, Writing – original draft. **Haowen Liu:** Investigation. **Hengcai Wu:** Investigation. **Qunqing Li:** Conceptualization, Supervision. **Yuegang Zhang:** Conceptualization, Supervision. **Shoushan Fan:** Conceptualization, Supervision. **Jiaping Wang:** Conceptualization, Supervision, Writing – review & editing.

Declaration of competing interest

The authors declare that they have no known competing financial interests or personal relationships that could have appeared to influence the work reported in this paper.

Acknowledgements

This work was supported by the National Basic Research Program of China (2019YFA0705702) and the National Natural Science Foundation of China (Grant Nos. 51872158 and 51532008).

Appendix A. Supplementary data

Supplementary data to this article can be found online at https://doi.org/10.1016/j.carbon.2021.02.075.

References

[1] M. Armand, J.-M. Tarascon, Building better batteries, Nature 451 (2008) 652–657, https://doi.org/10.1038/451652a.
[2] J.-M. Tarascon, M. Armand, Issues and challenges facing rechargeable lithium batteries, Nature 414 (2001) 359, https://doi.org/10.1142/9789814317665_0024.
[3] J. Xiao, How lithium dendrites form in liquid batteries. (New York, N.Y.), 366, 2019, pp. 426–427, https://doi.org/10.1126/science.aay8672, 6464.
[4] W. Xu, J. Wang, F. Ding, X. Chen, E. Nasybulin, Y. Zhang, J.-G. Zhang, Lithium metal anodes for rechargeable batteries, Energy Environ. Sci. 7 (2014) 513–537, https://doi.org/10.1039/C3EE40795K.
[5] G. Bieker, M. Winter, P. Bieker, Electrochemical in situ investigations of SEI and dendrite formation on the lithium metal anode, Phys. Chem. Chem. Phys. 17 (2015) 8670, https://doi.org/10.1039/c4cp05865h.
[6] J.-i. Yamaki, S.-i. Tobishima, K. Hayashi, K. Saito, Y. Nemoto, M. Arakawa, A consideration of the morphology of electrochemically deposited lithium in an organic electrolyte, J. Power Sources 74 (1998) 219–227, https://doi.org/10.1016/S0378-7753(98)00067-6.
[7] K.J. Harry, D.T. Hallinan, D.Y. Parkinson, A.A. MacDowell, N.P. Balsara, Detection of subsurface structures underneath dendrites formed on cycled lithium metal electrodes, Nat. Mater. 13 (2014) 69–73, https://doi.org/10.1038/nmat3793.
[8] R. Bhattacharyya, B. Key, H. Chen, A.S. Best, A.F. Hollenkamp, C.P. Grey, In situ NMR observation of the formation of metallic lithium microstructures in lithium batteries, Nat. Mater. 9 (2010) 504–510, https://doi.org/10.1038/nmat2764.
[9] H. Ota, K. Shima, M. Ue, J.-i. Yamaki, Effect of vinylene carbonate as additive to electrolyte for lithium metal anode, Electrochim. Acta 49 (2004) 565–572, https://doi.org/10.1016/j.electacta.2003.09.010.
[10] F. Ding, W. Xu, G.L. Graff, J. Zhang, M.L. Sushko, X. Chen, et al., Dendrite-free lithium deposition via self-healing electrostatic shield mechanism, J. Am. Chem. Soc. 135 (2013) 4450–4456, https://doi.org/10.1021/ja312241y.
[11] W. Li, H. Yao, K. Yan, G. Zheng, Z. Liang, Y.-M. Chiang, Y. Cui, The synergetic effect of lithium polysulfide and lithium nitrate to prevent lithium dendrite growth, Nat. Commun. 6 (2015) 7436, https://doi.org/10.1038/ncomms8436.
[12] S. Choudhury, R. Mangal, A. Agrawal, L.A. Archer, A highly reversible room-temperature lithium metal battery based on crosslinked hairy nanoparticles, Nat. Commun. 6 (2015) 10101, https://doi.org/10.1038/ncomms10101.
[13] F. Shen, M.B. Dixit, X. Xiao, K.B. Hatzell, Effect of pore connectivity on Li dendrite propagation within LLZO electrolytes observed with synchrotron X-ray tomography, ACS Energy Lett. 3 (4) (2018) 1056–1061, https://doi.org/10.1021/acsenergylett.8b00249.
[14] G. Zheng, S. Lee, Z. Liang, et al., Interconnected hollow carbon nanospheres for stable lithium metal anodes, Nat. Nanotechnol. 9 (2014) 618–623, https://doi.org/10.1038/nnano.2014.152.
[15] K. Yan, H.-W. Lee, T. Gao, G. Zheng, H. Yao, H. Wang, Z. Lu, Y. Zhou, Z. Liang, Z. Liu, S. Chu, Y. Cui, Ultrathin two-dimensional atomic crystals as stable interfacial layer for improvement of lithium metal anode, Nano Lett. 14 (10) (2014) 6016–6022, https://doi.org/10.1021/nl503125u.
[16] J. Pu, J. Li, K. Zhang, et al., Conductivity and lithiophilicity gradients guide lithium deposition to mitigate short circuits, Nat. Commun. 10 (2019) 1896, https://doi.org/10.1038/s41467-019-09932-1.
[17] S.-S. Chi, Y. Liu, W.-L. Song, L.-Z. Fan, Q. Zhang, Prestoring lithium into stable 3D nickel foam host as dendrite-free lithium metal anode, Adv. Funct. Mater. 27 (24) (2017) 1700348, https://doi.org/10.1002/adfm.201700348.
[18] Q. Li, S. Zhu, Y. Lu, 3D porous Cu current collector/Li-metal composite anode for stable lithium-metal batteries, Adv. Funct. Mater. 27 (18) (2017) 1606422, https://doi.org/10.1002/adfm.201606422.
[19] C.-P. Yang, Y.-X. Yin, S.-F. Zhang, N.-W. Li, Y.-G. Guo, Accommodating lithium into 3D current collectors with a submicron skeleton towards long-life lithium metal anodes, Nat. Commun. 6 (2015) 8058, https://doi.org/10.1038/ncomms9058.
[20] D. Lin, Y. Liu, Z. Liang, H.-W. Lee, J. Sun, H. Wang, K. Yan, J. Xie, Y. Cui, Layered reduced graphene oxide with nanoscale interlayer gaps as a stable host for lithium metal anodes, Nat. Nanotechnol. 11 (2016) 626, https://doi.org/10.1038/nnano.2016.32.
[21] W. Huang, Y. Yu, Z. Hou, et al., Dendrite-Free lithium electrode enabled by

graphene aerogels with gradient porosity, Energy Storage Mater. 33 (2020) 329–335, https://doi.org/10.1016/j.ensm.2020.08.032.
[22] G. Yang, Y. Li, Y. Tong, J. Qiu, S. Liu, S. Zhang, Z. Guan, B. Xu, Z. Wang, L. Chen, Lithium plating and stripping on carbon nanotube sponge, Nano Lett. 19 (1) (2019) 494–499, https://doi.org/10.1021/acs.nanolett.8b04376.
[23] Y. Luo, S. Luo, H. Wu, et al., Self-expansion construction of ultralight carbon nanotube Aerogels with a 3D and hierarchical cellular structure, Small 13 (28) (2017) 1700966, https://doi.org/10.1002/smll.201700966.
[24] Z. Fang, Y. Luo, H. Wu, et al., Mesoporous carbon nanotube aerogel-sulfur cathodes: a strategy to achieve ultrahigh areal capacity for lithium-sulfur batteries via capillary action, Carbon 166 (30) (2020) 183–192, https://doi.org/10.1016/j.carbon.2020.05.047.
[25] N. Shu, J. Xie, X. Wang, et al., Rolling press of lithium with carbon for high-performance anodes, Energy Storage Mater. 24 (2020) 689–693, https://doi.org/10.1016/j.ensm.2019.07.044.
[26] Z. Cao, B. Li, S. Yang, Dendrite-Free lithium anodes with ultra-deep stripping and plating properties based on vertically oriented lithium–copper–lithium arrays, Adv. Mater. 31 (29) (2019) 1901310.1–191901310, https://doi.org/10.1002/adma.201901310, 6.
[27] Z. Liang, D. Lin, J. Zhao, Z. Lu, Y. Liu, C. Liu, et al., Composite lithium metal anode by melt infusion of lithium into a 3D conducting scaffold with lithiophilic coating, Proc. Natl. Acad. Sci. Unit. States Am. 113 (11) (2016) 2862–2867, https://doi.org/10.1073/pnas.1518188113.
[28] B. Hong, H. Fan, X.-B. Cheng, X. Yan, S. Hong, Q. Dong, C. Gao, Z. Zhang, Y. Lai, Q. Zhang, Spatially uniform deposition of lithium metal in 3D Janus hosts, Energy Storage Mater. 16 (2019) 259–266, https://doi.org/10.1016/j.ensm.2018.04.032.
[29] C. Jin, O. Sheng, J. Luo, et al., 3D lithium metal embedded within lithiophilic porous matrix for stable lithium metal batteries, Nano Energy 37 (2017) 177–186, https://doi.org/10.1016/j.nanoen.2017.05.015.
[30] C. Sun, Y. Li, J. Jin, Z. Wen, ZnO nanoarray-modified nickel foam as a lithiophilic skeleton to regulate lithium deposition for lithium-metal batteries, J. Mater. Chem. A 7 (2019) 7752–7759, https://doi.org/10.1039/c9ta00862d.
[31] J. Sangster, C-Li (carbon-lithium) system, J. Phase Equilibria Diffus. 28 (2007) 561–570, https://doi.org/10.1007/s11669-007-9193-8.
[32] S. Luo, Y.F. Luo, H.C. Wu, M.Y. Li, L.J. Yan, K.L. Jiang, L. Liu, Q.Q. Li, S.S. Fan, J.P. Wang, Self-assembly of 3D carbon nanotube sponges: a simple and controllable way to build macroscopic and ultralight porous architectures, Adv. Mater. 29 (2017) 1603549, https://doi.org/10.1002/adma.201603549.
[33] K. Jiang, Q.Li S. Fan, Spinning continuous carbon nanotube yarns, Nature 419 (2002) 801, https://doi.org/10.1038/419801a.
[34] K. Liu, Y.H. Sun, L. Chen, C. Feng, X.F. Feng, K.L. Jiang, Y.G. Zhao, S.S. Fan, Controlled growth of super-aligned carbon nanotube arrays for spinning continuous unidirectional sheets with tunable physical properties, Nano Lett. 8 (2008) 700, https://doi.org/10.1021/nl0723073.
[35] K. Liu, K.L. Jiang, Y. Wei, S.P. Ge, P. Liu, S.S. Fan, Controlled termination of the growth of vertically aligned carbon nanotube Arrays, Adv. Mater. 19 (2007) 975, https://doi.org/10.1002/adma.200600600.
[36] M. Li, Y. Wu, F. Zhao, et al., Cycle and rate performance of chemically modified super-aligned carbon nanotube electrodes for lithium ion batteries, Carbon 69 (2014) 444–451, https://doi.org/10.1016/j.carbon.2013.12.047.
[37] J. Kang, H.-V. Kim, S./-A. Chae, K./-H. Kim, A new strategy for maximizing the storage capacity of lithium in carbon materials, Small 14 (2018) 1704394, https://doi.org/10.1002/smll.201704394.
[38] S.-H. Wang, J. Yue, W. Dong, et al., Tuning wettability of molten lithium via a chemical strategy for lithium metal anodes, Nat. Commun. 10 (2019) 4930, https://doi.org/10.1038/s41467-019-12938-4.
[39] X.-R. Chen, B.-Q. Li, C. Zhu, et al., A coaxial-interweaved hybrid lithium metal anode for long-lifespan lithium metal batteries, Adv. Energy Mater. 9 (39) (2019) 1901932, https://doi.org/10.1002/aenm.201901932.
[40] S. Liu, Y. Ma, Z. Zhou, et al., Inducing Uniform lithium nucleation by integrated lithium-rich li-in anode with lithiuophilic 3D framework, Energy Storage Mater. 33 (2020) 423–431, https://doi.org/10.1016/j.ensm.2020.08.007.
[41] C. Niu, H. Pan, W. Xu, et al., Self-smoothing anode for achieving high-energy lithium metal batteries under realistic conditions, Nat. Nanotechnol. 14 (2019) 594–601, https://doi.org/10.1038/s41565-019-0427-9.
[42] Y. Lu, Z. Tu, L.A. Archer, Stable lithium electrodeposition in liquid and nanoporous solid electrolytes, Nat. Mater. 13 (2014) 961–969, https://doi.org/10.1038/nmat4041.
[43] L. Yu, Q. Su, B. Li, et al., Bio-inspired lotus root-like 3D multichannel carbon hosts for stable lithium metal anodes, Electrochim. Acta 362 (2020) 137130, https://doi.org/10.1016/j.electacta.2020.137130.
[44] J. Sun, B. Li, C. Jin, et al., Construction of 3D porous CeO_2 ceramic hosts with enhanced lithiophilicity for dendtrite-free lithium metal anode, J. Power Sources 484 (2021) 229253, https://doi.org/10.1016/j.jpowsour.2020.229253.
[45] Y. Deng, H. Lu, Y. Cao, et al., Multi-walled carbon nanotube interlayers with controllable thickness for high-capacity and long-life lithium metal anodes, J. Power Sources 412 (2019) 170–179, https://doi.org/10.1016/j.jpowsour.2018.11.037.